

# Numerical storm surge model with higher order finite difference method of lines for the coast of Bangladesh

Gour Chandra Paul<sup>1\*</sup>, Md. Emran Ali<sup>2</sup>

<sup>1</sup> Department of Mathematics, University of Rajshahi, Rajshahi 6205, Bangladesh

<sup>2</sup> Department of Textile Engineering, Northern University Bangladesh, Dhaka 1230, Bangladesh

Received 31 January 2018; accepted 11 May 2018

© Chinese Society for Oceanography and Springer-Verlag GmbH Germany, part of Springer Nature 2019

## Abstract

In this study, the method of lines (MOLs) with higher order central difference approximation method coupled with the classical fourth order Runge-Kutta (RK(4,4)) method is used in solving shallow water equations (SWEs) in Cartesian coordinates to foresee water levels associated with a storm accurately along the coast of Bangladesh. In doing so, the partial derivatives of the SWEs with respect to the space variables were discretized with 5-point central difference, as a test case, to obtain a system of ordinary differential equations with time as an independent variable for every spatial grid point, which with initial conditions were solved by the RK(4,4) method. The complex land-sea interface and bottom topographic details were incorporated closely using nested schemes. The coastal and island boundaries were rectangularized through proper stair step representation, and the storing positions of the scalar and momentum variables were specified according to the rules of structured C-grid. A stable tidal regime was made over the model domain considering the effect of the major tidal constituent,  $M_2$  along the southern open boundary of the outermost parent scheme. The Meghna River fresh water discharge was taken into account for the inner most child scheme. To take into account the dynamic interaction of tide and surge, the generated tidal regime was introduced as the initial state of the sea, and the surge was then made to come over it through computer simulation. Numerical experiments were performed with the cyclone April 1991 to simulate water levels due to tide, surge, and their interaction at different stations along the coast of Bangladesh. Our computed results were found to compare reasonable well with the limited observed data obtained from Bangladesh Inland Water Transport Authority (BIWTA) and were found to be better in comparison with the results obtained through the regular finite difference method and the 3-point central difference MOLs coupled with the RK(4,4) method with regard to the root mean square error values.

**Key words:** shallow water equations, method of lines, higher order finite difference approximation method, surge, nested scheme

**Citation:** Paul Gour Chandra, Ali Md. Emran. 2019. Numerical storm surge model with higher order finite difference method of lines for the coast of Bangladesh. *Acta Oceanologica Sinica*, 38(6): 100–116, doi: 10.1007/s13131-019-1385-7

## 1 Introduction

Geographically, Bangladesh is situated at the interface of two important relatively opposite geographical constituents, namely ocean and hills (Ali and Choudhury, 2014). For such a type of junction, this area is highly favorable for different natural calamities, such as cyclones, storm surges, earthquakes, floods, droughts, etc. The Himalayas and Kashi-Jaintia hills, situated at the north and east of the country, respectively, are responsible for inland flooding by making monsoon rain and melting snow and ice through numerous rivers produced from their waterfall what make erosion of the river bank, create sedimentation and river migration, etc. On the other hand, the Bay of Bengal (BOB) is the source of various disasters, namely tropical cyclones (TCs) and associated surges, floods, salinity intrusion, coastal erosion, etc. Among the disasters, TCs and associated surges cause major devastation. It is documented that about five to six storms form every year in the BOB region but with about 80% of the global casualties (Debsarma, 2009). For making understand the ferocity of these storm surges along this region, Fig. 1 having different storm tracks and Table 1 with the corresponding losses are included. From Table 1 and Fig. 1, one can figure out the extent of losses

made by the surges associated with some notable tropical storms over the years and its impact on socioeconomic sectors. The coast of Bangladesh, located at the northern tip of the BOB, is recognized globally as the most vulnerable to cyclones and associated surges (Paul et al., 2017). The reasons behind the vulnerability are the complex coastline, thickly populated offshore islands of different shapes, shallow bathymetry, huge discharge through the Meghna River and other rivers, high tidal range, etc. We cannot prevent storm surges, but we can better be prepared for it. However, this can best be done by increasing awareness among the coastal people through a proper warning system and such a system is highly dependent on an accurate storm surge prediction model. Bangladesh Meteorological Department (BMD) has a warning system based on a numerical model brought from the IIT Kharagpur, India, which is a surge model and can predict the landfall time, sea level rising as well as the storm track in a certain accuracy (Debsarma, 2009). But the predictions by the storm warning center meteorologists of the BMD in terms of the precise location of cyclones, landfall timing, precise estimation of surge height, etc. have often been criticized (Hossain et al., 2008). Thus an appeal is emerged to the research community for the de-

\*Corresponding author, E-mail: [pcgour2001@yahoo.com](mailto:pcgour2001@yahoo.com)

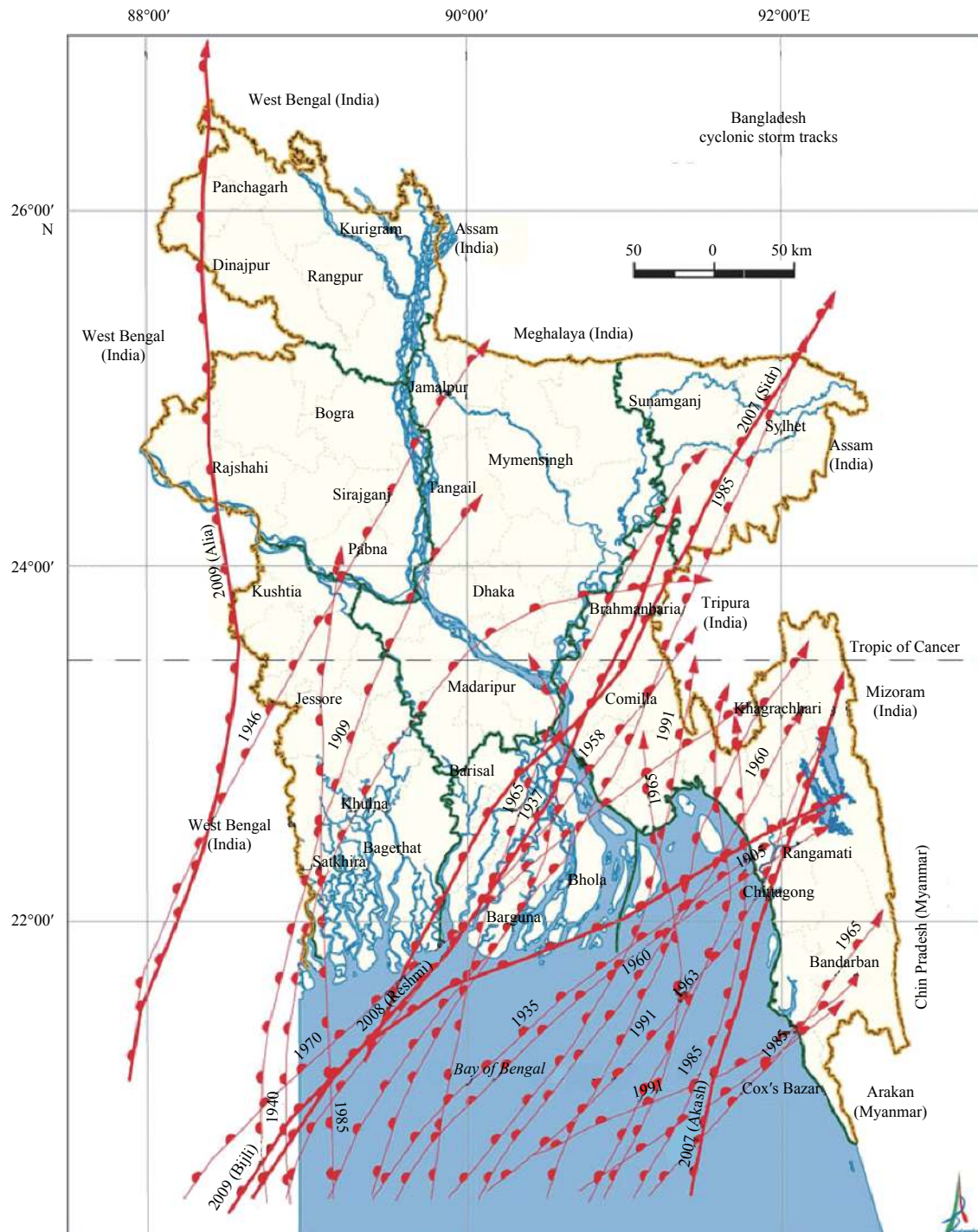


**Fig. 1.** The northwest corner of the Bay of Bengal and tracks of several cyclones (source: Banglapedia).

velopment of a proper storm surge prediction model for the region executable in the existing system of the country.

A large volume of works (Das, 1972; Johns and Ali, 1980; Roy, 1995, 1999a, b; Paul and Ismail, 2012a, b, 2013; Paul et al., 2016, 2017, 2018a, b) have been made in this region in order to develop a proper warning system. Among them, the pioneering work due to Das (1972) was conducted by the FDM considering the linear interaction of tide and surge with stair step representation of the complex land-sea interface with a low resolution of grids. But tide is a continuous process in the sea and hence it will always interact with surge nonlinearly (Johns and Ali, 1980).

However, Johns and Ali (1980) solved one of the problems mentioned above taking into account the nonlinear interaction of tide and surge. But the study due to Johns and Ali (1980) was also limited to ensuring an improved resolution of grids. It is known that the accuracy of the results from a model using stair step approximation of coasts highly depends on the choice of grid resolution (Paul et al., 2016). Hence, the results obtained in the study of Johns and Ali (1980) may differ somewhat from the actual situation (Paul et al., 2016). All other studies based on the stair step representation, specially Roy (1995, 1999a, b), Paul and Ismail (2012a, b, 2013) and Paul et al. (2016, 2017) were conducted by

**Table 1.** Landfall locations and losses of life due to storm surges (data sources: [Debsarma \(2009\)](#) and NASA website)

Year	Location of landfall	Human death
1970	Bangladesh	500 000
1897	Bangladesh	175 000
1991	Bangladesh	140 000
1876	Bangladesh	100 000
1822	Bangladesh	40 000
1965	Bangladesh	19 279
1963	Bangladesh	11 520
1961	Bangladesh	11 468
1977	India	10 000
1960	Bangladesh	5 149
2007	Bangladesh	3 376
2009	India	275
2016	Bangladesh	24

the FDM with the goal of getting benefits in computational cost and in the accuracy of the results including different surge affecting factors. But in FDM, one cannot get the benefit in computational cost as well as in the accuracy in computed results at the same time due to the maintenance of the Courant-Friedrichs-Lewy (CFL) stability criterion. In this respect, the study due to [Paul et al. \(2014\)](#) is an alternative one, where a new approach, the method of lines (MOLs) in coordination with the RK(4,4) method was adopted for solving SWEs in storm surge simulation. Later, the study due to [Paul et al. \(2014\)](#) was reinvestigated by [Paul et al. \(2018a, b\)](#) to obtain computational efficiency. It is to be noted here that [Ismail et al. \(2007\)](#) firstly used the technique to simulate Indonesian tsunami 2004 along the west coast of Peninsular Malaysia and Thailand. However, in the mentioned groups of investigations, the adopted discretization method for spatial derivatives was 3-point central difference (3PCD). It is of interest to note here that higher order finite difference approximation increases the accuracy of a model result ([Chapra and Canale, 2015](#)). With this goal, a different approach, a higher order central difference MOLs coupled with the RK(4,4) method is adopted in this study to foresee water levels during storm surges along the coast of Bangladesh. The present study is thus an improvement over the study of [Paul et al. \(2014\)](#) who used the 3PCD MOL in coordination with the RK(4,4) method, where the complexities of the coast were incorporated with relatively low resolution of grids. Also, it is our intention to see how the results obtained through the different approach compare some observed data and reported results and to see whether the present study can be a serious alternative of the existing ones conducted with a rigorous treatment of the problem.

The rest of the paper is organized as follows. Section 2 deals with the higher order central difference MOLs. The problem statement is stated in Section 3 and in its subsections. Numerical procedure is described in detail in Section 4 and in its subsections. Section 5 deals with the model results, their discussion and model validation. Finally, conclusion is presented in Section 6.

## 2 Method of lines with higher order central difference approximation

Typically, the MOLs is a semi-analytic method that converts partial differential equations (PDEs) into a set of ordinary differential equations (ODEs) discretizing all variables related to the derivatives using finite difference approximations leaving one continuous ([Pregla, 1987; Pregla and Pascher, 1989; Sadiku, 2000](#)), whereas, generally, the time derivatives, if exist, are kept

continuous. Over the several years, the method makes good popularity to the research community due to having some benefits, especially, in computational cost, stability criterion, and simplicity in solving PDEs ([Schuesser and Griffiths, 2009; Bakodah, 2011; Paul et al., 2014](#)).

As a higher order finite difference approximation method, in our study, we have used 5-point central difference (5PCD) approximation in the following form ([Rehman and Taj, 2009, 2011; Rehman et al., 2014](#)):

$$\frac{du(x)}{dx} = au(x-2h) + bu(x-h) + cu(x) + du(x+h) + eu(x+2h), \quad (1)$$

where  $a$ ,  $b$ ,  $c$ ,  $d$  and  $e$  are constants to be determined. The values of the constants can be determined from the solution of a set of algebraic equations generated by equating the terms on the right hand side with the left one of Eq. (1) obtained from Taylor series expansion. Substituting the values of the constants in Eq. (1), one can see it to the form:

$$\frac{du(x)}{dx} = \frac{1}{12h} (u(x-2h) - 8u(x-h) + 8u(x+h) - u(x+2h)). \quad (2)$$

The approximation specified by Eq. (2) is implemented in the model equations for their discretizations.

## 3 Problem statement

### 3.1 Model equations

The vertically integrated SWEs for the dynamical process in the sea can be given by ([Paul and Ismail, 2013; Paul et al., 2014, 2018a, b](#))

$$\frac{\partial \zeta}{\partial t} = -\frac{\partial}{\partial x} [(\zeta+h)u] - \frac{\partial}{\partial y} [(\zeta+h)v], \quad (3)$$

$$\frac{\partial u}{\partial t} = -u \frac{\partial u}{\partial x} - v \frac{\partial u}{\partial y} + f v - g \frac{\partial \zeta}{\partial x} + \frac{T_x}{\rho(\zeta+h)} - C_f \frac{u(u^2+v^2)^{\frac{1}{2}}}{\zeta+h}, \quad (4)$$

$$\frac{\partial v}{\partial t} = -u \frac{\partial v}{\partial x} - v \frac{\partial v}{\partial y} - f u - g \frac{\partial \zeta}{\partial y} + \frac{T_y}{\rho(\zeta+h)} - C_f \frac{v(u^2+v^2)^{\frac{1}{2}}}{\zeta+h}, \quad (5)$$

where  $x$  and  $y$  represent the coordinate axes directed towards the south and the east, respectively, with the reference point ( $23^\circ\text{N}$ ,  $85^\circ\text{E}$ ) on the mean sea level at the north-west corner of the study domain;  $u$  and  $v$  symbolize the Reynold's averaged velocity components in  $x$ - and  $y$ -directions, respectively;  $h(x, y)$  denotes the undisturbed water depth and  $\zeta(x, y, t)$  stands for denoting the elevation of the free surface at any point over time  $t$  about the undisturbed surface level;  $f = 2\Omega \sin \phi$  is the Coriolis parameter, where  $\Omega$  represents the angular speed of the earth rotation and  $\phi$  is the latitude of the place of interest;  $g$  is the acceleration due to local gravity;  $\rho$  denotes the density of sea water;  $C_f$

the friction coefficient;  $T_x$  and  $T_y$  stand for the components of wind stress acting on the water surface along  $x$  and  $y$  directions, respectively.

In this study, the surface stresses are parameterized using a conventional quadratic law (Jelesnianski, 1965):

$$(T_x, T_y) = \rho_a C_D \sqrt{(u_a^2 + v_a^2)} (u_a, v_a), \quad (6)$$

where  $C_D$  is the surface drag coefficient, which varies with the wind speed and the stability of the atmosphere (Das et al., 1974). In our study, we have used  $C_D = 0.0028$ , which is found to be used by most modelers (Das, 1972);  $\rho_a$  is the density of the air; and  $u_a$ ,  $v_a$  are the velocity components of the surface wind in  $x$ - and  $y$ -directions, respectively. Though there are various empirical formulae for generating wind stress depending upon the meteorological information, we have adopted the formula due to Jelesnianski (1965), being given by

$$V_a = \begin{cases} V_0 \sqrt{\left(\frac{r_a}{R}\right)^3} & \text{for all } r_a < R, \\ V_0 \sqrt{\left(\frac{R}{r_a}\right)^3} & \text{for all } r_a > R, \end{cases} \quad (7)$$

where  $V_0$  is the maximum sustained wind speed and  $R$  is the corresponding radial distance from the eye of the storm;  $r_a$  represents the radial distance at which the wind field is to be generated. It is to be noted here that the meteorological information that are required in generating the wind field led by the formula mentioned above are available in BMD. The generation of wind field led by the above formula over the region of interest can be found to be supported by various studies (Roy, 1995, 1999a; Paul and Ismail, 2012a; Paul et al., 2014, 2016, 2018a).

### 3.2 Boundary conditions

There are two types of boundaries, namely closed and open boundaries. The coastal belt (northern boundary) and island boundaries are treated as the closed boundaries, where the normal component of the Reynold's depth-averaged velocity is assumed to be zero. The other three boundaries are treated as open boundaries, where the effects of different factors are required to be included depending upon the availability of the data and specific modelling application (Mills, 1985). Due to unavailability of sufficient information, in most of the studies conducted over the BOB region, a radiation type boundary condition is found to use for the open boundaries (Roy, 1995), which allows internally generated disturbances to propagate outwards normally across the open boundaries without disturbing them (Sinha et al., 1986). In our study, the following open boundary conditions are used (Paul and Ismail, 2012b, 2013):

the west boundary:

$$v + \sqrt{\frac{g}{h}} \zeta = 0; \quad (8)$$

the east boundary:

$$v - \sqrt{\frac{g}{h}} \zeta = 0; \quad (9)$$

the south boundary:

$$u - \sqrt{\frac{g}{h}} \zeta = -2a \sqrt{\frac{g}{h}} \sin\left(\frac{2\pi t}{T} + \varphi\right), \quad (10)$$

where  $a$  and  $\varphi$  denote the prescribed amplitude and phase, respectively, of the tidal constituent of interest, and  $T$  denotes its period.

Along the northern boundary of the innermost child scheme, as we will see later, Meghna River is considered between longitudes  $90.46^\circ\text{E}$  and  $90.61^\circ\text{E}$  along latitude  $23^\circ\text{N}$  and following Roy (1995), the river fresh water discharge is taken into account by the formula:

$$u_b = u + \frac{Q}{B(h + \zeta)}, \quad (11)$$

where  $Q$  is the fresh water discharge through the river, and  $B$  is the breadth of the river, which is approximately 16 km in width at the mentioned position.

## 4 Numerical procedure

### 4.1 Set-up of nested scheme

The study domain (Fig. 2) of interest is extended from latitudes  $15^\circ$  to  $23^\circ\text{N}$  and longitudes  $85^\circ$  to  $95^\circ\text{E}$ . The reason behind the consideration of such a big domain is that it is required for keeping the storm at least for three days on the domain, which is prerequisite to make people aware of the situation along the coastal region (Rahman et al., 2017). To incorporate the complex land-sea interface and bottom topographic details, a high resolution of grid is required. But the use of such an improved grid resolution over such a big domain increases the computational cost tremendously. In order to solve this fact, following Paul et al. (2016), one-way nested grid technique is used in this study. The coarse mesh scheme (CMS) is the parent one extended over the whole domain of interest with relatively lower resolution (Fig. 3). It is to be noted here that in the deep sea, the elevation of sea surface is rarely affected by the factors mentioned above (Paul et al., 2016). But they are highly effective on surge towards the coast (Paul and Ismail, 2013; Paul et al., 2016, 2017). Therefore, a fine mesh scheme (FMS) with a relatively high resolution (Fig. 3) is nested into the CMS covering the whole coastal region of the country. The FMS is designed in such a way that it can be able to incorporate the coastal complexities and the effect of islands properly except that of the Meghna deltaic region. Here the mouth of the Meghna River falls into the sea and the sedimentation and fresh water discharge through the river are changing the topography of the sea bed continuously. So in this area, an extra care is needed to be taken into account, which is made sure with the nesting of another very fine mesh scheme (VFMS) into the FMS (Fig. 3). A detailed description of the three schemes is presented in Table 2, whereas Fig. 2 may help to make understand the study domain with nested schemes. The coupling of the schemes is made by the process used in Paul et al. (2016).

### 4.2 Discretization of special derivatives

The governing equations specified by Eqs (3)–(5) along with the boundary conditions prescribed by Eqs (8)–(10) are discretized with the aid of Eq. (2) providing the discrete points in the computational  $xy$ -plane defined by  $x_i = (i - 1)\Delta x$ ,  $i = 1, 2, 3, \dots, M$  (even) and  $y_j = (j - 1)\Delta y$ ,  $j = 1, 2, 3, \dots, N$  (odd) using the staggered C-grid in which there are three distinct types of computational points. With  $i$  even and  $j$  odd, the point is a  $\zeta$ -

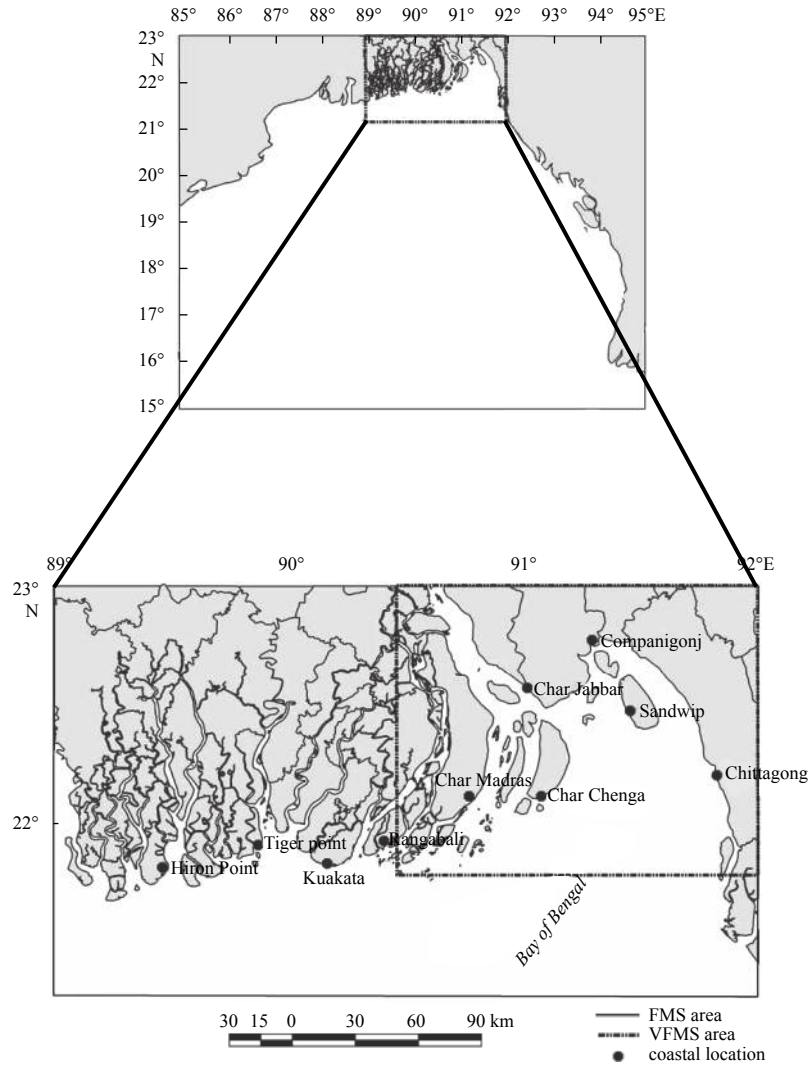


**Fig. 2.** Domain of the study area with doubly nested schemes (after Paul et al. (2016)).

point at which  $\zeta$  is computed. If  $i$  and  $j$  both are odd, the point is a  $u$ -point at which  $u$  is computed and if  $i$  and  $j$  both are even, the point is a  $v$ -point at which  $v$  is computed.  $M$  and  $N$  are chosen to be even and odd, respectively, to ensure  $\zeta$  and  $v$  points along the southern open sea boundary and  $\zeta$  and  $u$  points along the eastern and western open sea boundaries. It is to be noted here that to discretize model equations by finite difference approximation method, the domain should be rectangularized. Stair step method can be of help in this regard. A fictitious coastal boundary and its stair step representation on an Arakawa C-grid are shown in Fig. 4 for better understanding. It is pertinent to point out here that in approximating the complex land-sea interface on the Arakawa C-grid, following the rule of stair step representation, we used our developed MATLAB routine. Our approximated coastal and island boundaries after imposing stair step method on the different schemes are shown in Fig. 3, which show incorporation of the coastal complexities differently in different schemes. However, after the discretizations, the continuity equation and the  $x$  and  $y$  components of the momentum equation can be written in the following forms:

For every grid point  $(x_i, y_j)$ , where  $i = 2, 4, 6, \dots, M - 2$ ,  $j = 1, 3, 5, \dots, N - 2$ , and Eq. (3) can be written as

$$\left(\frac{\partial \zeta}{\partial t}\right)_{i,j} = f_1(\zeta_{l,m}^k, u_{l,m}^k, v_{l,m}^k, h_{l,m}), \quad (12)$$

where  $l = i - 3, i - 2, i - 1, i, i + 1, i + 2, i + 3$ ;  $m = j - 3, j - 2, j - 1, j, j + 1, j + 2, j + 3$ .

Similarly, for every grid point  $(x_i, y_j)$ , where  $i = 3, 5, 7, \dots, M - 1$ ,  $j = 3, 5, 7, \dots, N - 2$ , and the  $x$ -component of momentum equation specified by Eq. (4) can be set to the following form:

$$\left(\frac{\partial u}{\partial t}\right)_{i,j} = f_2(\zeta_{l,m}^{k+1}, u_{l,m}^k, v_{l,m}^k, h_{l,m}), \quad (13)$$

where  $l = i - 3, i - 2, i - 1, i, i + 1, i + 2, i + 3$ ; and  $m = j - 3, j - 2, j - 1, j, j + 1, j + 2, j + 3$ .

Finally, for the grid point  $(x_i, y_j)$ , where  $i = 2, 4, 6, \dots, M - 2$ , and  $j = 2, 4, 6, \dots, N - 1$ ,  $y$ -component of momentum equation specified by Eq. (5) can be written as

$$\left(\frac{\partial v}{\partial t}\right)_{i,j} = f_3(\zeta_{l,m}^{k+1}, u_{l,m}^k, v_{l,m}^k, h_{l,m}), \quad (14)$$

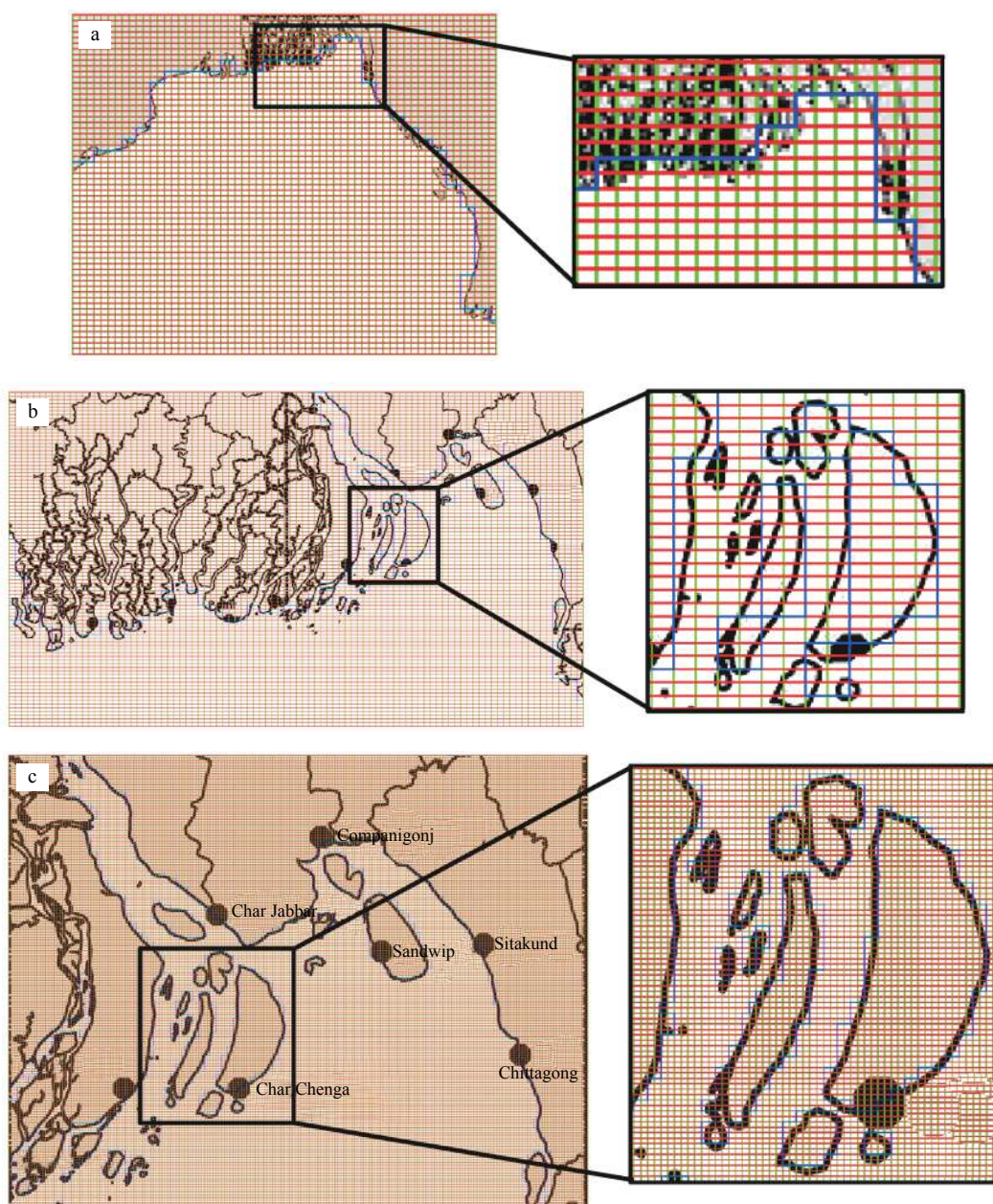


**Fig. 3.** Grids of the schemes, CMS, FMS and VFMS and approximated coastal and island boundaries through stair step representation in the respective scheme with enlarged view at the right of each of the schemes for a portion. a. CMS, b. FMS and c. VFMS. These schemes are similar to those of Paul et al. (2016).

**Table 2.** Details about the nested schemes

Scheme	Domain	Step size along $x$ -axis	Step size along $y$ -axis	Number of grid points
CMS	15°–23°N, 85°–92°E	15.08 km	17.52 km	60 × 61
FMS	21°15′–23°N, 89°–92°E	2.15 km	3.29 km	92 × 95
VFMS	21.77°–23°N, 90.40°–92°E	720.73 m	1 142.39 m	190 × 145

where  $l = i - 3, i - 2, i - 1, i, i + 1, i + 2, i + 3$ ; and  $m = j - 3, j - 2, j - 1, j, j + 1, j + 2, j + 3$ .

In the above equations, the prefix  $k$  means that the values of the variables are at the current time level and  $k + 1$  means that the values of the variables are at the advanced time level.

#### 4.3 The data sources and used numerical values

In order to run the model, some data are to be allocated as in-

put data including oceanographical, meteorological, hydrological, and geographical. To specify the water depth data accurately to the grids discussed in Section 4.1, the area covering our domain is cropped from Fig. 3, which was used in the study of Johns et al. (1985). Then by a MATLAB routine, a matrix with water depth information specified by the given contours is produced. Depth information at the remaining elements of the matrix is generated using Shepard interpolation. A contour map of our interpolated

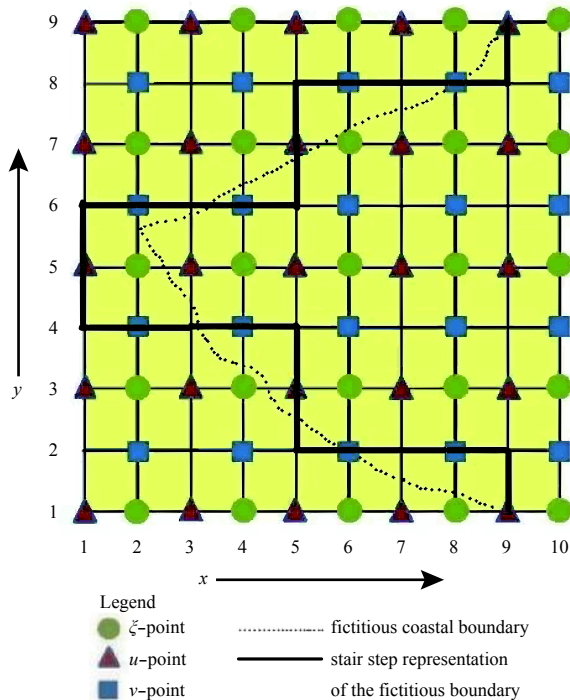


**Fig. 4.** The used staggered Arakawa C-grid system with a fictitious coastal or island boundary and its stair step representation.

bathymetry is shown in Fig. 5. The bathymetric data at each of the longitudinal and latitudinal positions of the computational grid points of the CMS, FMS and VFMS are then compiled from the generated matrix using again the Shepard interpolation. The meteorological inputs namely, storm track, maximum sustained wind speed and maximum wind radius are collected from the BMD and in this regard, Table 3 and Fig. 6 are included for better understanding. The rotation speed of the earth and density of the sea water are taken as  $\Omega = 1\,040$  m/h, and  $\rho = 1\,025$  kg/m<sup>3</sup> (Paul et al., 2014), respectively. The value of the friction coefficient  $C_f$  is taken as constant for computational simplicity, which is 0.0026. The tidal period is taken as  $T = 12.4$  h (Roy, 1995). Initial values of the momentum and scalar variables are taken as

zero to represent an initial state of static equilibrium, which is supported by the studies due to Loy et al. (2014) and Paul et al. (2016, 2018a, b). It is to be mentioned here that the mentioned initial state is the best assumption; otherwise, the real values of  $\zeta$ ,  $u$  and  $v$  have to be made available at all grid points in the region of analysis (Loy et al., 2014). The time step is taken as  $\Delta t = 60$  s that ensured CFL stability criterion.

#### 4.4 Solution procedure

The obtained discretized equations given by Eqs (12)–(14) are solved with the RK(4,4) method.

First, Eq. (12) with the initial conditions and the defined values of the parameters involved (Appendix, Eq. (A1)) is solved by the RK(4,4) method for the values of  $\zeta$ . A detailed description of the solution procedure can be found in Paul et al. (2014). After getting the values of  $\zeta$  at the points specified by the Arakawa C-grid, its values are calculated at the specified grids of the boundaries through Eqs (A3)–(A5) (Appendix) and then averaging procedure is taken into account to obtain  $\zeta$  at each of the grid points representing water, coastal and island boundaries. Path of the storm is then generated with the obtained data from the BMD (Table 3) and the wind field is generated subsequently with the values of the required parameters from the BMD with the help of Eqs (6) and (7). Equation (13) is then solved with the help of the RK(4,4) method. Finally, Eq. (14) is solved for the  $y$ -component of momentum equation. The procedure mentioned above is made for all the schemes. The only difference is in the boundaries as is mentioned earlier. The Meghna River fresh water discharge is incorporated in the northern open boundary of the VFMS using Eq. (A6) at the points  $(1, j)$  where  $j = 7, 9, 11, 13, 15, 17, 19$ . This procedure is repeated over time supplying the updated values as initial ones for calculating water levels due to tide, surge, and their interaction. It is pertinent to point out here that for generating a stable tidal regime over the model domain, the model was run setting the initial conditions to zero, known as "cold start" in the absence of atmospheric pressure gradient force and wind stress. First, the values of amplitude ( $a$ ) and phase ( $\varphi$ ) related to the  $M_2$  tidal constituent are prescribed in Eq. (10) along the southern open boundary of the CMS from the study of McCammon and Wunsch (1977). The period of the tidal oscillation  $T$  is taken as 12.4 h, as the mean period is always found to be approximately 12.4 h, which is of  $M_2$  tide. Then from the cold start in the

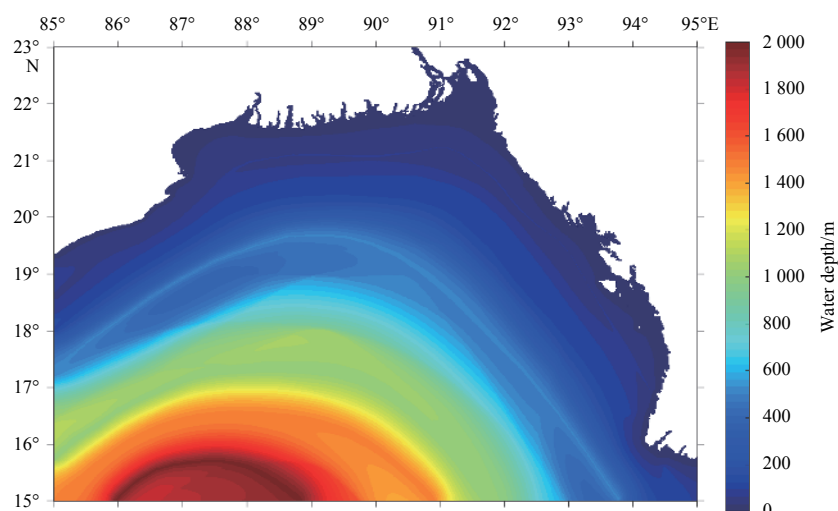


**Fig. 5.** Our generated bathymetric figure through Shepard interpolation.

**Table 3.** Time series for the positions and nature of the cyclone April 1991 (data sources: BMD)

Date (1991)	Hour (UTC)	North latitude	East longitude	Nature of the storm
Apr. 26	1800	11.80°	87.50°	cyclonic storm
Apr. 27	0300	12.50°	87.50°	cyclonic storm
Apr. 27	0600	13.00°	87.50°	cyclonic storm
Apr. 27	0900	13.60°	87.50°	severe cyclonic storm
Apr. 27	1800	14.50°	87.50°	severe cyclonic storm with hurricane core
Apr. 28	0600	15.80°	87.70°	severe cyclonic storm with hurricane core
Apr. 28	0800	16.50°	88.00°	severe cyclonic storm with hurricane core
Apr. 28	1800	17.60°	88.30°	severe cyclonic storm with hurricane core
Apr. 29	0600	19.80°	89.40°	severe cyclonic storm with hurricane core
Apr. 29	1200	20.80°	90.40°	severe cyclonic storm with hurricane core
Apr. 29	1800	22.00°	91.40°	severe cyclonic storm with hurricane core
Apr. 29	2000	22.30°	91.80°	crossing the coast near Chittagong
Apr. 30	0000	23.00°	92.40°	crossed the Bangladesh coast
Apr. 30	0200	23.50°	92.80°	

Note: Maximum sustained wind speed: 234 km/h and maximum radius of sustained wind: 50 km.

absence of wind field, a stable tidal regime is achieved after four cycles of integration. But the problem to generate a pure oscillatory response in the BOB region corresponding to the tidal constituent with period  $T$  lies with adjustment of the exact values of  $a$  and  $\varphi$ . Thus some techniques are needed to be adopted for precise specification of the values of the constants and in this regards, we use the technique of Roy (1995) to adjust the values of  $a$  and  $\varphi$ . Generation of a stable tidal condition by the process along the area of interest is supported by several studies (Johns et al., 1985; Roy, 1995, 1999b; Paul and Ismail, 2012b, 2013; Paul et al., 2016). For the pure surge (in the absence of astronomical tide), the model was also run from the cold start. It pertinent to pinpoint out here that the zero initial values will not affect the calculated results as their effect on the results over several hours will almost disappear (Zhang et al., 2007). For estimating water levels due to the interaction of tide and surge, the generated pure tidal regime provided the initial condition at the model time  $t = 0$ .

#### 4.5 Cyclone arrival time and its characteristics

The numerical experimentations were carried out with the cyclone April 1991. The reasons behind the choice of the cyclone are that it was a severe one and it passed nearby the Meghna River mouth, the region of our interest. Also, the investigated information about the cyclone is relatively more. The cyclone was so ferocious that about 150 000 people and 70 000 cattle were died having an economical loss of about Tk 80 billion (Khalil, 1992). For discussions of our model simulated results, the time history of the storm is utmost urgent. A detailed description of the time history of the storm can be found in Paul et al. (2016, 2017, 2018a), therefore, a gist of it is presented here for convenience. The cyclone was first detected as a depression on 23 April 1991 from the satellite pictures taken at Space Research and Remote Sensing Organization (SPARRSO) from National Oceanic and Atmospheric Administration (NOAA)-II and Geostationary Meteorological Satellite-4 (Khalil, 1993). It was gradually propagated towards the coast gaining energy. At 0300 universal time coordinate (UTC) of 25 April, it was identified as a deep depression near (10°N, 89°E). The depression was gradually intensified and at 0300 UTC of 28 April, it was detected at (15.5°N, 87.5°E) having central speed of 30 m/s. Suddenly it changed its direction and started moving easterly towards the estuary of Meghna River. Finally, it hit the coast of Bangladesh near Chittagong along Noakhali coast at 2000 UTC of 29 April. The maximum sustained

wind speed 65 m/s of the storm was examined at Sandwip.

#### 5 Results and discussion

The program was executed for 80 h from 1800 UTC of 26 April to 0200 UTC of 30 April and the results were displayed for the last 48 h from 0200 UTC of 28 April to 0200 UTC of 30 April.

Figure 7 depicts our model simulated tidal results at different coastal stations (Fig. 2) splitting the domain of interest into three coastal plains, namely the Ganges tidal plain, the Meghna deltaic plain and the Chittagong straight plain. It can be seen from Fig. 7 that the five coastal stations along the Ganges tidal plain exhibit about the same tidal characters, whereas in the other two plains, amplitudes and phases of the tides are found to be varied. Our simulated time variation of astronomical tides with respect to the mean sea level at Hiron Point, Char Chenga (Hatiya) and Chittagong with the tidal data obtained from the BIWTA are presented in Fig. 8. It can be inferred from the figure that our simulated astronomical tides are in a reasonable agreement with the tidal data obtained from the BIWTA. The reason behind the choice of the stations is that the accessibility of data is comparatively more at those three stations over the other locations.

Our simulated water levels due to pure surge at different coastal locations are depicted in the same way as mentioned above in Fig. 9. It can be seen from Fig. 9 that at the five stations included in the Ganges tidal plain, resurgent happened faster relative to the stations included in the other coastal plains. It may be a result of surge negative impact of the mangrove forest. Among the stations included in the Meghna deltaic plain, the resurgent happened slowly. The reason behind the happening may be that during surges, waters were migrated through the numerous rivers situated in this plain (Figs 1 and 2) and hence they came back slowly when resurgent occurred. But in the Chittagong straight plain, we could not find such types of impacts but resurgent occurred comparatively faster here due to the direct hit of surge with the straight shore line of the plain. The maximum and minimum peak surge heights were estimated to be 4.09 m and 3.23 m at Tiger point and Kuakata, respectively, in the Ganges tidal plain. In the Meghna deltaic plain, the peak surge heights were found to vary between 3.74 m (Chitalkhali) and 5.98 m (Companigonj), whereas along the Chittagong deltaic plain, the peak surge values were found to range from 2.10 m (Cox's Bazar) to 5.09 m (Mirsarai). However, the peak surge levels along the coast were found to vary between 2.10 m (Cox's Bazar) and 5.98 m

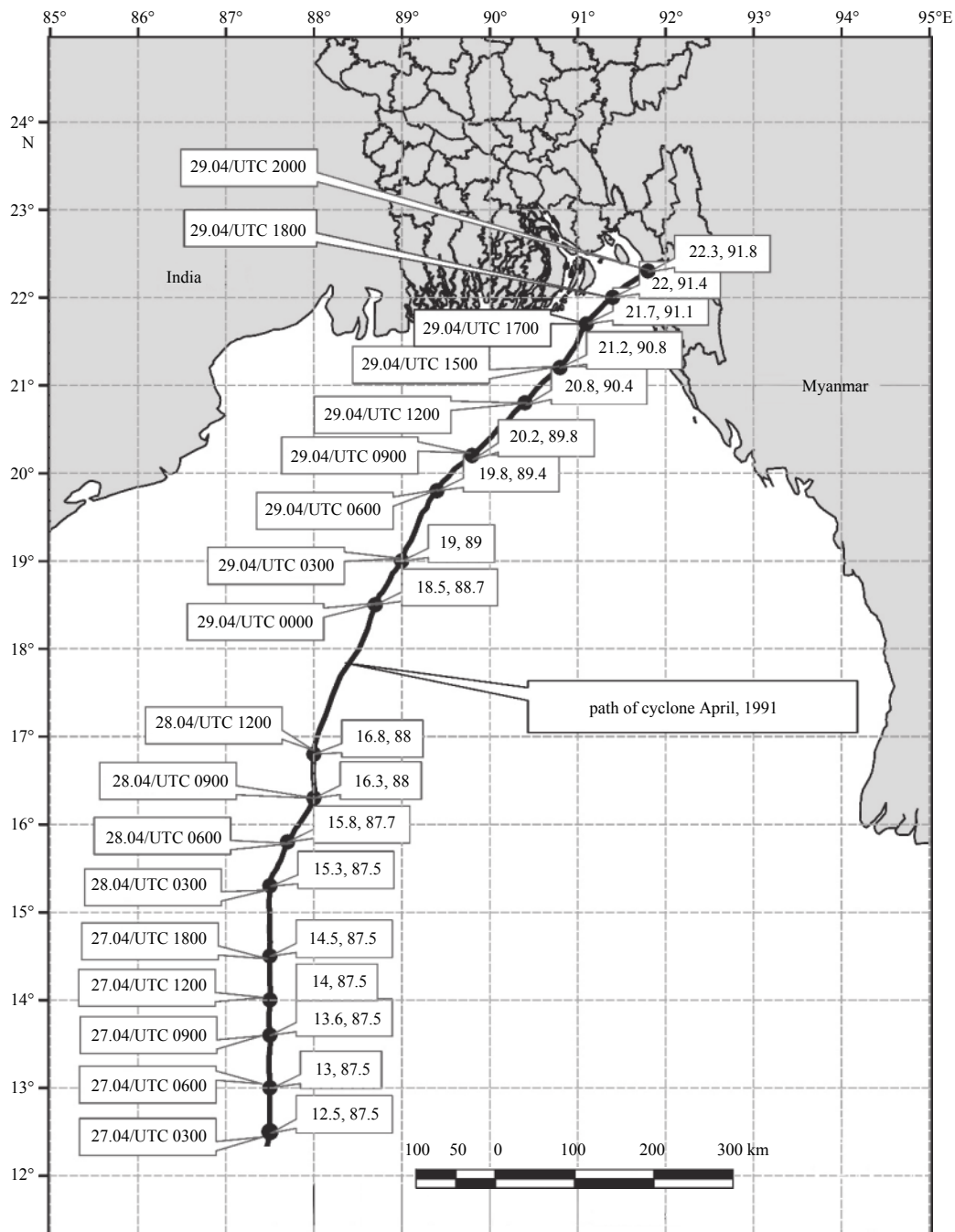


**Fig. 6.** Observed track of the cyclonic storm April 1991 (after Paul et al. (2016)). The numbers in the left such as 29.04/UTC 2000 mean the time is 2000 UTC of 29 April; and the numbers in the right such as 22.3, 91.8 indicate the location is 22.3°N, 91.8°E.

(Companigonj), which agree fairly well with the results obtained in Paul and Ismail (2012a, 2013), Paul et al. (2014, 2016, 2017, 2018a). Figure 10 shows simulated total water levels obtained from the study with the nonlinear interaction of tide and surge presented in the same way mentioned above. From Fig. 10, it can be inferred that the peak total water levels came out through our simulation vary between 2.05–6.78 m with maximum 6.78 m at Companigonj. Flather (1994), in his investigation, also found the highest total water level (7.21 m) on the Noakhali coast. Thus, our simulated peak total water level at Noakhali coast (6.78 m) compares well with the corresponding result found in Flather (1994).

For the validation of the model results and for making clear

the idea of interaction phenomena, our computed water levels due to tide, surge, their interaction and superposition are presented with observed water levels during the mentioned period of displaying results in Fig. 11 choosing the three stations Hiron Point, Char Chenga and Chittagong from each of the mentioned coastal plains. We chose the same stations for a reason mentioned before. However, it can be perceived from Fig. 11 that our computed results due to the interaction of tide and surge compare reasonably well with the observed data from the BIWTA. It can also be seen from Fig. 11 that the water levels that came out through the superposition of tide and surge are in agreement with observed data. Thus with the superposition of tide and

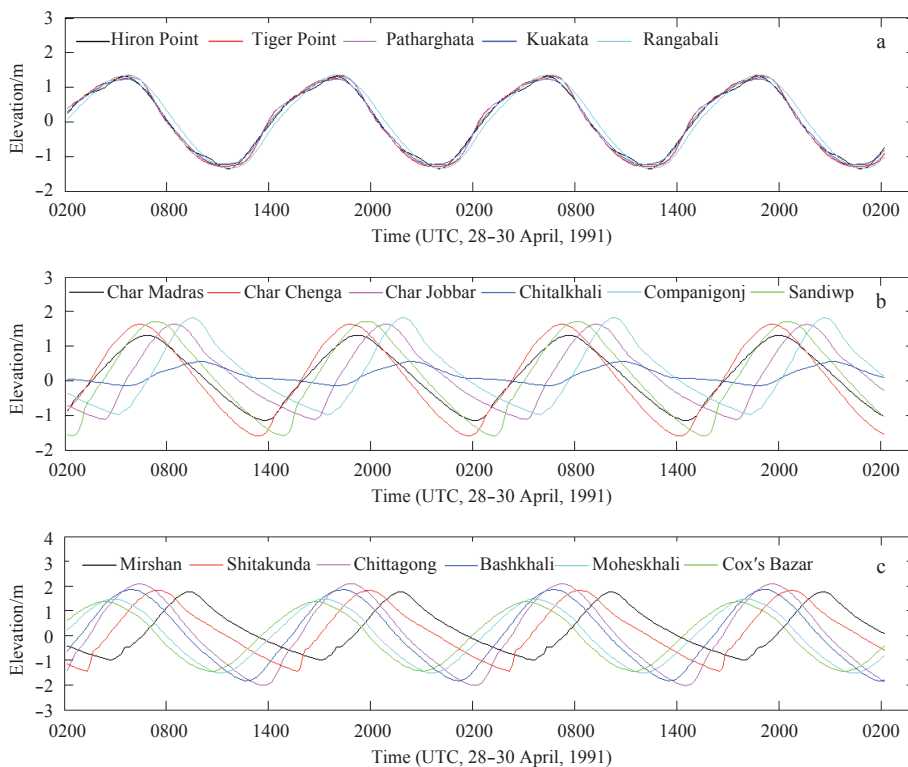


**Fig. 7.** Computed time variation of astronomical tide with respect to the MSL for the chosen period of displaying results in different coastal stations along the Ganges tidal plain (a), the Meghna deltaic plain (b), and the Chittagong straight plain (c).

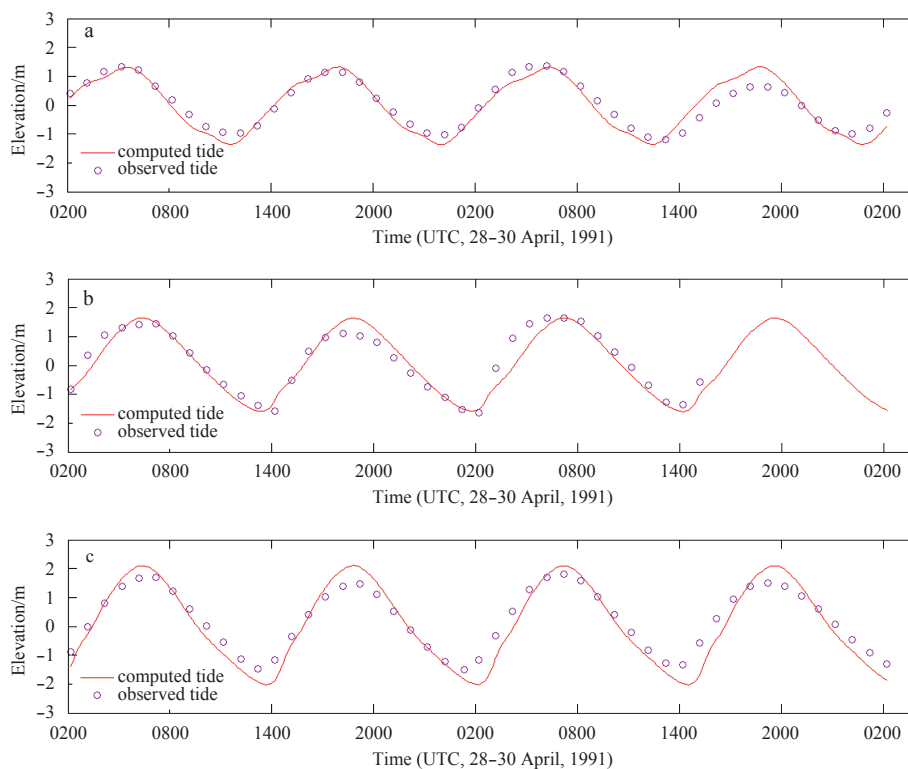


**Fig. 8.** Comparison of our simulated time variation of astronomical tides with respect to the MSL with the tidal data obtained from the BIWTA for the chosen period of displaying results at Hiron Point (a), Char Chenga (b) and Chittagong (c). In each case, a solid curve represents the configuration for our computed tidal levels, and a circle represents a tidal data at that moment obtained from the BIWTA.

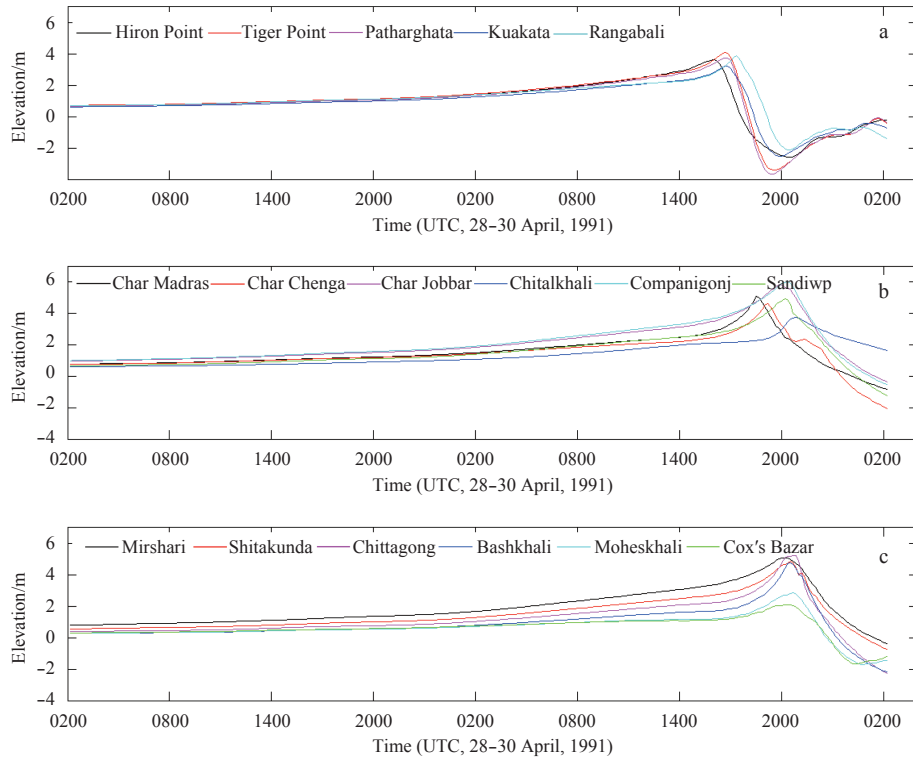


**Fig. 9.** Computed time variation of pure surge levels (in the absence of astronomical tide) with respect to the MSL at different coastal stations; along the Ganges tidal plain (a), the Meghna deltaic plain (b), and the Chittagong straight plain (c).

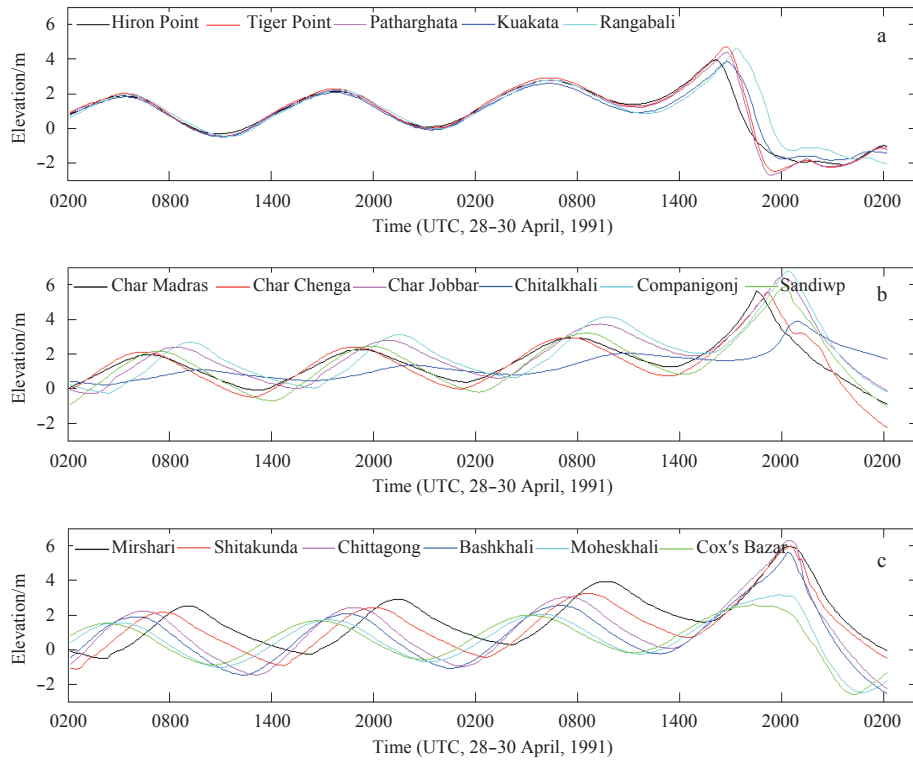


**Fig. 10.** Computed time variation water levels with respect to the MSL due to the dynamical interaction of tide and surge associated with the storm April 1991 at seventeen coastal stations along the Ganges tidal plain (a), the Meghna deltaic plain (b), and the Chittagong straight plain (c).

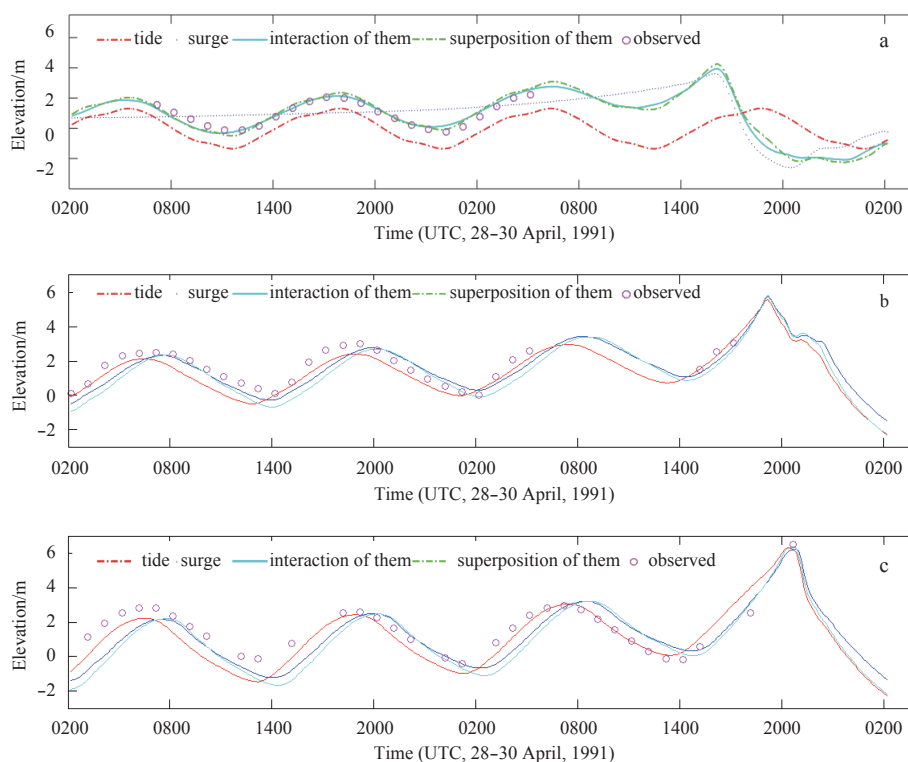


**Fig. 11.** The time variation of water levels with respect to the MSL due to tide, surge, their interaction and superposition with observed data obtained from the BIWTA at Hiron Point (a), Char Chenga (b) and Chittagong (c). We have almost used all the observed data set obtained in the mentioned period.

surge, a rough estimation on total water levels can be made. But, in actuality, tide is a continuous process in the sea and it will always interact with tide nonlinearly.

Our model simulated results are also presented with the results obtained by the FDM (Paul and Ismail, 2012a) and 3PCD MOLs in coordination with the RK(4,4) method (Paul et al., 2014) in Fig. 12, whereas peak surge levels and peak total water levels are presented in Table 4 for better understanding and for making a comparison to show the effectiveness of the model results. It can be inferred from Fig. 12 and Table 4 that the obtained results from the study are reasonable and are found to compare well with the results obtained with the 3-point regular FDM and the 3PCD MOL in coordination with the RK(4,4) method.

We have tested the effect of the dynamic interaction of tide and surge at the seventeen coastal locations. To test this effect, as in Paul et al. (2016), total water level  $\zeta$  was represented as the sum of the water levels due to tide, water levels due to the pure storm surge produced by the meteorological conditions only, and the residual elevation (interaction effect) due to tide and surge interaction (Paul et al., 2016). The effects of the dynamic interaction of tide and surge are depicted in Fig. 13. It can be observed from Fig. 13 that a considerable interaction between tides and surges occurs at some stations. The maximum effect is found at Chittagong of about 1.9 m. The water levels due to the interaction of tide and surge is found to be less than the water levels due to pure surge at times of high tide and greater than the water levels due to surge alone at times of low tide, and consequently the peak values of total water levels consistently occur after the time of high tide except when the storm is nearer to the coast, where tide can be found to be dominated by surge (Fig. 11). However, a considerable change in amplitude and phase can be

found to be produced along the Meghna estuarine region due to the interaction effect (Figs 11 and 13). Thus the interaction effect may affect the timing of peak water levels during storm events. Therefore, it is crucial to understand and incorporate the tide and surge interaction along the coast of Bangladesh for the precise forecasting of storm surges in coastal defense.

The efficiency of the results obtained in the study is also tested with respect to the root means square error (RMSE) values and are presented in Table 5. The expression for RMSE is

$$\text{RMSE} = \sqrt{\frac{1}{N} \sum_{i=1}^N (X_{\text{obs},i} - X_{\text{model},i})^2}, \text{ where } X_{\text{obs},i} \text{ and } X_{\text{model},i}$$

are observed and modelled values at time  $i$ , respectively, and  $n$  represents the size of the sample. We have also presented the RMSE values of the results obtained by the FDM and 3PCD MOLs with the RK(4,4) method and the results obtained in some variety of investigations (Roy et al., 1999; Paul et al., 2016, 2017) in Table 5. The RMSE values were calculated with observed data and the model simulated results in the said period. It is found from Table 5 that our model results can be acceptable and found to be better over the FDM and 3PCD MOLs in coordination with the RK(4,4) method with regard to the RMSE values.

For testing the flexibility of the method adopted in the present study, we run the present model as well as the models by the FDM and 3PCD MOLs with the RK(4,4) method in estimating total water levels with different time steps, namely 10 s, 30 s, 90 s and 120 s. The FDM failed to yield results for some of the chosen time steps. Thus MOLs technique can be found to be flexible as it may process a stable solution flexibly maintaining the CFL stability criteria. For testing computational efficiency, each of the mentioned models was run on the same computer (Intel® Core™ i5-7500 Processor) in estimating total water levels with time step 60 s.

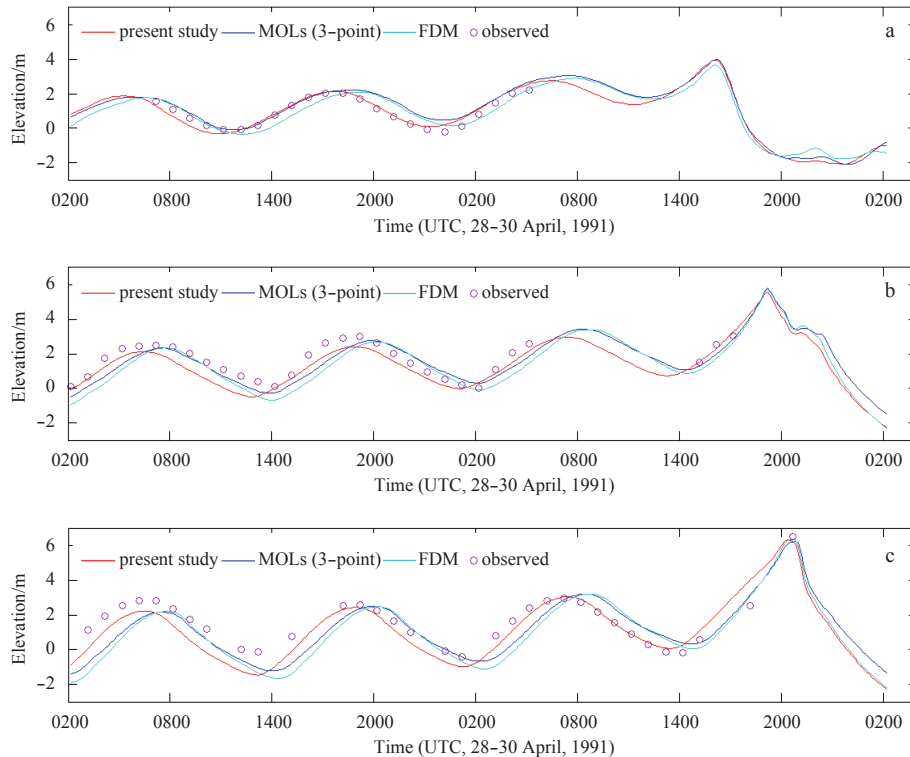


**Fig. 12.** Comparison of our computed water levels due to the interaction of tide and surge simulated by the present study with those obtained by the 3PCD MOLs with the RK(4,4) method and FDM with observed data at Hiron Point (a), Char Chenga (b) and Chittagong (c).

**Table 4.** Comparison of our computed peak water levels simulated by the present study with respect to the mean sea level (MSL) and those obtained by the 3PCD MOLs in coordination with the RK(4,4) method and FDM

Coastal location	Present study		MOLs (3-point)		FDM	
	Simulated max surge level/m	Total peak water level/m	Simulated max surge level/m	Total peak water level/m	Simulated max surge level/m	Total peak water level/m
Hiron Point	3.61	3.95	3.92	4.01	3.88	3.37
Tiger Point	4.09	4.71	4.21	4.57	4.24	4.42
Patharghata	3.76	4.38	3.97	3.01	3.91	4.09
Kuakata	3.23	3.85	3.52	3.86	3.45	3.62
Rangabali	3.91	2.23	4.10	4.50	4.14	4.34
Char Madras	5.05	5.62	5.50	5.81	5.60	5.85
Char Chenga	4.61	5.58	5.11	5.81	5.27	5.90
Char Jabbar	5.79	6.45	6.19	6.35	6.32	6.40
Chitalkhali	3.74	3.87	4.64	4.42	4.96	4.68
Companigonj	5.98	6.78	6.70	7.28	7.10	7.21
Sandwip	4.93	5.89	5.24	5.63	5.43	5.73
Mirsharai	5.09	5.98	5.50	4.61	5.77	5.40
Sita Kunda	4.48	6.02	4.83	5.78	5.13	5.93
Chittagong	5.22	6.30	5.17	6.26	5.39	6.55
Banshkhali	4.78	5.61	5.03	6.10	4.98	3.12
Moheskhali	2.88	3.17	3.13	3.77	2.90	3.84
Cox's Bazar	2.10	2.59	2.12	2.65	2.09	2.99

In the case of the present study, we need a little bit more computational time over the other two methods. But the computational cost can be reduced here with the proper choice of the time step. The time step 60 s was chosen as it was suitable to run all the said models. Therefore, based on the model simulated results, we may say that the present study is an effective and efficient one in the prediction of storm surges along the region of interest. It is to be mentioned that water levels for the region of interest are af-

ected by several factors (Paul et al., 2016) with the coastal complexities may be the main one but we did not present them in the case of the present study as the main focus of the study is to get benefit from computation and to see whether the study can be a suitable alternative of the existing ones for having efficient results. However, the effects of surge affecting factors can be found to present in Paul et al. (2016).

In our simulated storm surge magnitude, there may have un-

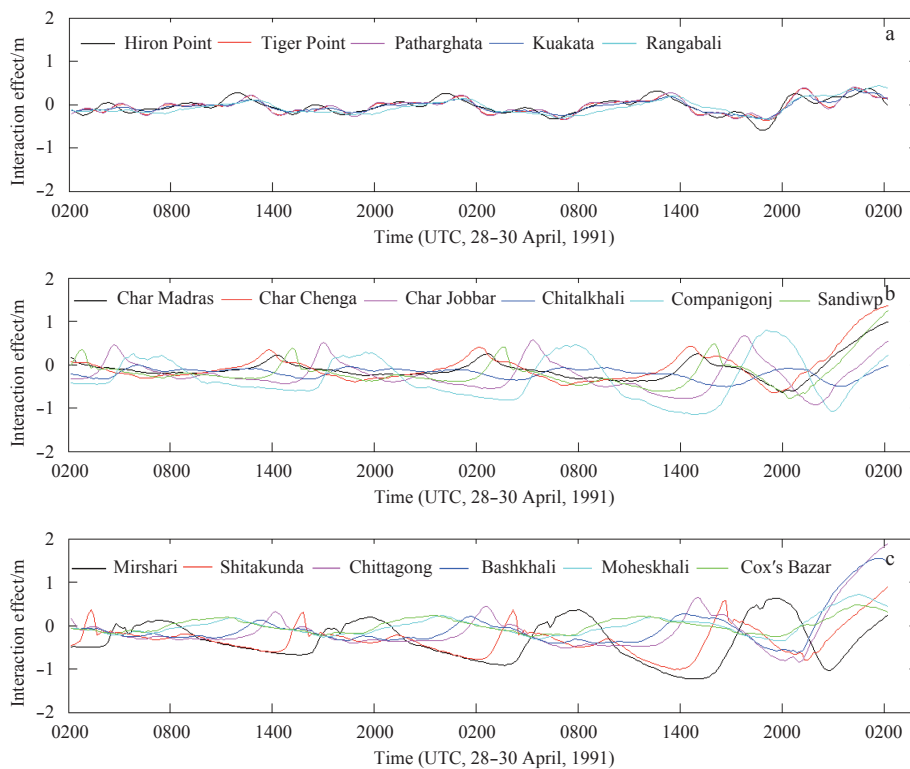


**Fig. 13.** Computed time variation of interaction effect associated with the storm April 1991 at seventeen coastal stations along Ganges tidal plain (a), Meghna deltaic plain (b), and Chittagong straight plain (c).

**Table 5.** Estimated RMSE values in metre by the present study, 3PCD MOLs with the RK(4,4) method and FDM at Hiron Point, Char Chenga, and Chittagong

Coastal station	The present study	MOLs (3-point)	FDM	The study due to Paul et al.			The study due to Roy et al. (1999)
				(2014)	(2016)	(2017)	
Hiron Point	0.05	0.32	0.03	0.39	0.16	0.32	0.49
Char Chenga	0.38	0.38	0.58	0.46	0.58	0.65	0.78
Chittagong	0.25	0.32	0.48	0.57	0.73	0.73	0.67

Note: The errors have been estimated between observed and computed water levels. We used almost all the data in the chosen period.

certainty, which can arise from bathymetry data, track of the cyclone, maximum sustained wind speed, and the maximum sustained wind radius (Madsen and Jakobsen, 2004; Lewis et al., 2014; Paul et al., 2016). As in Paul et al. (2016), uncertainties concerned with each of these factors have been estimated with freely available data sources retaining the other factors remained fixed. The result in our computed water level magnitude came out to be  $\sim 0.4$  m, which is comparable to the prediction accuracy of water levels (Table 5). It is to be noted at this juncture that uncertainties from freely available data sources may be very high (Lewis et al., 2013).

## 6 Conclusions

In this study, a cyclone-induced storm surge model with a higher order central difference MOLs, in specific, a 5PCD MOLs in coordination with the RK(4,4) method has been developed to foresee water level accurately along the coast of Bangladesh. The developed model is applied to simulate water levels due to the interaction of tide and surge associated with the tropical storm April 1991 at some coastal stations of Bangladesh. The model-simulated results are found to be in a reasonable agreement with the observed data from the BIWTA and with the results obtained by the 3PCD MOLs with the RK(4,4) method and FDM. The mod-

el is found to be more flexible in storm surge simulation over the FDM with regard to stability and can be found to be suitable over both the 3PCD MOLs coupled with the RK(4,4) method and FDM in terms of accuracy. Also, computational cost in the case of the present study can be reduced with the choice of suitable time step. Thus based on the different approach adopted in the study, an effective storm surge prediction model can be established. A sophisticated time integrator may make the present study a more effective one, where one can also use a higher order (7 or 9) central difference MOLs for more efficient results.

## Acknowledgements

The first author thanks Sujit Kumar Debsarma for his valuable discussion about the data sources. We thank Mizanur Rahman from Sylhet University of Science and Technology for providing necessary data. The second author thanks Aslam Hossain, lecturer, Department of Applied Mathematics, Gono University, Savar, Dhaka, Bangladesh for his kind help during editing the manuscript.

## References

Ali A, Choudhury G A. 2014. Storm Surges in Bangladesh: An Introduction to CEGIS Storm Surge Model. Dhaka, Bangladesh: The

University Press Limited

- Bakodah H O. 2011. Non-central 7-point formula in the method of lines for parabolic and Burgers' equations. *International Journal of Research and Reviews in Applied Sciences*, 8(3): 328–336
- Chapra S C, Canale R P. 2015. *Numerical Methods for Engineers*. 7th ed. New York, USA: McGraw-Hill, Inc
- Das P K. 1972. Prediction model for storm surges in the Bay of Bengal. *Nature*, 239(5369): 211–213, doi: [10.1038/239211a0](https://doi.org/10.1038/239211a0)
- Das P K, Sinha M C, Balasubramanyam V. 1974. Storm surges in the Bay of Bengal. *Quarterly Journal of the Royal Meteorological Society*, 100(425): 437–449
- Debsarma S K. 2009. Simulations of storm surges in the Bay of Bengal. *Marine Geodesy*, 32(2): 178–198, doi: [10.1080/01490410902869458](https://doi.org/10.1080/01490410902869458)
- Flather R A. 1994. A storm surge prediction model for the northern Bay of Bengal with application to the cyclone disaster in April 1991. *Journal of Physical Oceanography*, 24(1): 172–190, doi: [10.1175/1520-0485\(1994\)024<0172:ASSPMF>2.0.CO;2](https://doi.org/10.1175/1520-0485(1994)024<0172:ASSPMF>2.0.CO;2)
- Hossain M Z, Islam M T, Sakai T, et al. 2008. Impact of tropical cyclones on rural infrastructures in Bangladesh. *Agricultural Engineering International: the CIGR Ejournal*, 2: 1–13
- Ismail A I M, Karim F, Roy G D, et al. 2007. Numerical modelling of tsunami via the method of lines. *World Academy of Science, Engineering and Technology*, 32: 177–185
- Jelesnianski C P. 1965. A numerical calculation of storm tides induced by a tropical storm impinging on a continental shelf. *Monthly Weather Review*, 93(6): 343–358, doi: [10.1175/1520-0493\(1993\)093<0343:ANCOS>2.3.CO;2](https://doi.org/10.1175/1520-0493(1993)093<0343:ANCOS>2.3.CO;2)
- Johns B, Ali M A. 1980. The numerical modelling of storm surges in the Bay of Bengal. *Quarterly Journal of the Royal Meteorological Society*, 106(447): 1–18, doi: [10.1002/\(ISSN\)1477-870X](https://doi.org/10.1002/(ISSN)1477-870X)
- Johns B, Rao A D, Dube S K, et al. 1985. Numerical modelling of tide-surge interaction in the Bay of Bengal. *Philosophical Transactions of the Royal Society A*, 313(1526): 507–535, doi: [10.1098/rsta.1985.0002](https://doi.org/10.1098/rsta.1985.0002)
- Khalil G M. 1992. Cyclones and storm surges in Bangladesh: some mitigative measures. *Natural Hazards*, 6(1): 11–24, doi: [10.1007/BF00162096](https://doi.org/10.1007/BF00162096)
- Khalil G M. 1993. The catastrophic cyclone of April 1991: its impact on the economy of Bangladesh. *Natural Hazards*, 8(3): 263–281, doi: [10.1007/BF00690911](https://doi.org/10.1007/BF00690911)
- Lewis M, Bates P, Horsburgh K, et al. 2013. A storm surge inundation model of the northern Bay of Bengal using publicly available data. *Quarterly Journal of the Royal Meteorological Society*, 139(671): 358–369, doi: [10.1002/qj.2040](https://doi.org/10.1002/qj.2040)
- Lewis M, Horsburgh K, Bates P. 2014. Bay of Bengal cyclone extreme water level estimate uncertainty. *Natural Hazards*, 72(2): 983–996, doi: [10.1007/s11069-014-1046-2](https://doi.org/10.1007/s11069-014-1046-2)
- Loy K C, Sinha P C, Liew J, et al. 2014. Modeling storm surges associated with super typhoon dorian in South China Sea. *Natural Hazards*, 70(1): 23–37, doi: [10.1007/s11069-010-9674-7](https://doi.org/10.1007/s11069-010-9674-7)
- Madsen H, Jakobsen F. 2004. Cyclone induced storm surge and flood forecasting in the northern Bay of Bengal. *Coastal Engineering*, 51(4): 277–296, doi: [10.1016/j.coastaleng.2004.03.001](https://doi.org/10.1016/j.coastaleng.2004.03.001)
- McCannon C, Wunsch C. 1977. Tidal charts of the Indian Ocean North of 15°S. *Journal of Geophysical Research*, 82(37): 5993–5998, doi: [10.1029/JC082i037p05993](https://doi.org/10.1029/JC082i037p05993)
- Mills D A. 1985. A numerical hydrodynamic model applied to tidal dynamics in the Dampier Archipelago. *Bulletin No. 190*. Western Australia: Department of Conservation and Environment
- Paul G C, Ismail A I M. 2012a. Numerical modeling of storm surges with air bubble effects along the coast of Bangladesh. *Ocean Engineering*, 42: 188–194, doi: [10.1016/j.oceaneng.2012.01.006](https://doi.org/10.1016/j.oceaneng.2012.01.006)
- Paul G C, Ismail A I M. 2012b. Tide-surge interaction model including air bubble effects for the coast of Bangladesh. *Journal of the Franklin Institute*, 349(8): 2530–2546, doi: [10.1016/j.jfranklin.2012.08.003](https://doi.org/10.1016/j.jfranklin.2012.08.003)
- Paul G C, Ismail A I M. 2013. Contribution of offshore islands in the prediction of water levels due to tide-surge interaction for the coastal region of Bangladesh. *Natural Hazards*, 65(1): 13–25, doi: [10.1007/s11069-012-0341-z](https://doi.org/10.1007/s11069-012-0341-z)
- Paul G C, Ismail A I M, Karim M F. 2014. Implementation of method of lines to predict water levels due to a storm along the coastal region of Bangladesh. *Journal of Oceanography*, 70(3): 199–210, doi: [10.1007/s10872-014-0224-x](https://doi.org/10.1007/s10872-014-0224-x)
- Paul G C, Ismail A I M, Rahman A, et al. 2016. Development of tide-surge interaction model for the coastal region of Bangladesh. *Estuaries and Coasts*, 39(6): 1582–1599, doi: [10.1007/s12237-016-0110-4](https://doi.org/10.1007/s12237-016-0110-4)
- Paul G C, Murshed M M, Haque M R, et al. 2017. Development of a cylindrical polar coordinates shallow water storm surge model for the coast of Bangladesh. *Journal of Coastal Conservation*, 21(6): 951–966, doi: [10.1007/s11852-017-0565-x](https://doi.org/10.1007/s11852-017-0565-x)
- Paul G C, Senthilkumar S, Pria R. 2018a. Storm surge simulation along the Meghna estuarine area: an alternative approach. *Acta Oceanologica Sinica*, 37(1): 40–49, doi: [10.1007/s13131-018-1157-9](https://doi.org/10.1007/s13131-018-1157-9)
- Paul G C, Senthilkumar S, Pria R. 2018b. An efficient approach to forecast water levels owing to the interaction of tide and surge associated with a storm along the coast of Bangladesh. *Ocean Engineering*, 148: 516–529, doi: [10.1016/j.oceaneng.2017.10.031](https://doi.org/10.1016/j.oceaneng.2017.10.031)
- Pregla R. 1987. About the nature of the method of lines. *Archiv für Elektronik und Übertragungstechnik*, 41(6): 368–370
- Pregla R, Pascher W. 1989. The method of lines. In: Itoh T, ed. *Numerical Techniques for Microwave and Millimeter-Wave Passive Structures*. New York: John Wiley, 381–446
- Rahman M M, Paul G C, Hoque A. 2017. A shallow water model for computing water level due to tide and surge along the coast of Bangladesh using nested numerical schemes. *Mathematics and Computers in Simulation*, 132: 257–276, doi: [10.1016/j.matcom.2016.08.007](https://doi.org/10.1016/j.matcom.2016.08.007)
- Rehman M A, Taj M S A. 2009. Fourth-order method for non-homogeneous heat equation with nonlocal boundary conditions. *Applied Mathematical Sciences*, 3(37): 1811–1821
- Rehman M A, Taj M S A. 2011. A numerical technique for heat equation subject to integral specifications. *Science International (Lahore)*, 24(1): 1–6
- Rehman M A, Taj M S A, Mardan S A. 2014. Fifth order numerical method for heat equation with nonlocal boundary conditions. *Journal of Mathematical and Computational Science*, 4(6): 1044–1054
- Roy G D. 1995. Estimation of expected maximum possible water level along the Meghna estuary using a tide and surge interaction model. *Environment International*, 21(5): 671–677, doi: [10.1016/0160-4120\(95\)00078-Y](https://doi.org/10.1016/0160-4120(95)00078-Y)
- Roy G D. 1999a. Inclusion of off-shore islands in a transformed coordinates shallow water model along the coast of Bangladesh. *Environment International*, 25(1): 67–74, doi: [10.1016/S0160-4120\(98\)00094-4](https://doi.org/10.1016/S0160-4120(98)00094-4)
- Roy G D. 1999b. Sensitivity of water level associated with tropical storms along the Meghna estuary in Bangladesh. *Environment International*, 25(1): 109–116, doi: [10.1016/S0160-4120\(98\)00095-6](https://doi.org/10.1016/S0160-4120(98)00095-6)
- Roy G D, Kabir A B M H, Mandal M M, et al. 1999. Polar coordinates shallow water storm surge model for the coast of Bangladesh. *Dynamics of Atmospheres and Oceans*, 29(2–4): 397–413, doi: [10.1016/S0377-0265\(99\)00012-3](https://doi.org/10.1016/S0377-0265(99)00012-3)
- Sadiku M N O, Garcia R C. 2000. Method of lines solution of axisymmetric problems. In: *Proceedings of 2000 IEEE Southeastcon*. Nashville, TN, USA: IEEE, 527–530
- Schiesser W E, Griffiths G W. 2009. *A Compendium of Partial Differential Equation Models: Method of Lines Analysis with Matlab*. Cambridge: Cambridge University Press
- Sinha P C, Dube S K, Roy G D, et al. 1986. Numerical simulation of storm surges in Bangladesh using a multi-level model. *International Journal for Numerical Methods in Fluids*, 6(5): 305–311, doi: [10.1002/\(ISSN\)1097-0363](https://doi.org/10.1002/(ISSN)1097-0363)
- Zhang Wenzhou, Hong Huasheng, Shang Shaoping, et al. 2007. A two-way nested coupled tide-surge model for the Taiwan Strait. *Continental Shelf Research*, 27(10–11): 1548–1567, doi: [10.1016/j.csr.2007.01.018](https://doi.org/10.1016/j.csr.2007.01.018)

## Appendix:

If  $\chi(x_i, y_j, t)$  be any dependent variable at any grid points  $(x_i, y_j)$ , at time  $t_k$ , then it can be discretized on spatial variables remaining one continuous as follows. The operators used in our discretization are given below.

$$\begin{aligned}\chi(x_i, y_j, t_k) &= \chi_{i,j}^k, \quad \frac{1}{2}(\chi(x_{i+1}, y_j, t^k) + \chi(x_{i-1}, y_j, t^k)) = \overline{\chi_{i,j}^k}^x, \\ \frac{1}{2}(\chi(x_i, y_{j+1}, t^k) + \chi(x_i, y_{j-1}, t^k)) &= \overline{\chi_{i,j}^k}^y, \\ \frac{1}{4}(\chi(x_{i+1}, y_{j+1}, t^k) + \chi(x_{i+1}, y_{j-1}, t^k) &+ \chi(x_{i-1}, y_{j+1}, t^k) + \chi(x_{i-1}, y_{j-1}, t^k)) = \overline{\chi_{i,j}^k}^{xy}.\end{aligned}$$

On the discretization of Eq. (3), one can see

$$\left(\frac{\partial \zeta}{\partial t}\right)_{i,j} = CR1 + CR2, \quad (A1)$$

where  $i = 2, 4, 6, \dots, M - 2i$  and  $j = 3, 5, 7, \dots, N - 2$ .

$$\text{In Eq. (A1), } CR1 = -\frac{1}{12 \Delta x} (z_1 - 8z_2 + 8z_3 - z_4), \quad CR2 = -\frac{1}{12 \Delta y} (z_5 - 8z_6 + 8z_7 - z_8),$$

where

$$\begin{aligned}z_1 &= \begin{cases} (\zeta_{i-2,j}^k + h_{i-2,j}) \overline{u_{i-2,j}^k}^x, & \text{if } i \neq 2, \\ (3 \zeta_{i,j}^k - 2 \zeta_{i+2,j}^k + 1.25 h_{i-1,j} - 0.25 h_{i,j}^k)(3 u_{i-1,j}^k - 2 \zeta_{i+1,j}^k), & \text{otherwise,} \end{cases} \\ z_2 &= \begin{cases} (\overline{\zeta_{i-1,j}^k}^x + h_{i-2,j}) u_{i-1,j}^k, & \text{if } i \neq 2, \\ (1.25 \zeta_{i,j}^k - 0.25 \zeta_{i+2,j}^k + h_{i-1,j}^k) u_{i-1,j}^k, & \text{otherwise,} \end{cases} \\ z_3 &= (\overline{\zeta_{i+1,j}^k}^x + h_{i+1,j}) u_{i+1,j}^k, \\ z_4 &= \begin{cases} (\zeta_{i+2,j}^k + h_{i+2,j}) \overline{u_{i+2,j}^k}^x, & \text{if } i \neq M - 2, \\ (\zeta_{i+2,j}^k + h_{i+2,j}^k)(1.25 u_{i+1,j}^k - 0.25 u_{i-1,j}^k), & \text{otherwise,} \end{cases} \\ z_5 &= \begin{cases} (\zeta_{i,j-2}^k + h_{i,j-2}) \overline{v_{i,j-2}^k}^y, & \text{if } j \neq 3, \\ (\zeta_{i,j-2}^k + h_{i,j-2})(3 v_{i,j-1}^k - 2 v_{i,j+1}^k), & \text{otherwise,} \end{cases} \\ z_6 &= (\overline{\zeta_{i,j-1}^k}^y + h_{i,j-1}) u_{i,j-1}^k, z_7 = (\overline{\zeta_{i,j+1}^k}^y + h_{i,j+1}) u_{i,j+1}^k, \\ z_8 &= \begin{cases} (\zeta_{i,j+2}^k + h_{i,j+2}) \overline{v_{i,j+2}^k}^y, & \text{if } j \neq 3, \\ (\zeta_{i,j+2}^k + h_{i,j+2})(1.25 v_{i,j+1}^k - 0.25 v_{i,j-1}^k), & \text{otherwise.} \end{cases}\end{aligned}$$

After discretizing Eq. (4), one can bring it to the following form:

$$\left(\frac{\partial u}{\partial t}\right)_{i,j} = UR1 + UR2 + UR3 + UR4 + UR5 + UR6, \quad (A2)$$

where  $i = 3, 5, 7, \dots, M - 1$  and  $i = 3, 5, 7, \dots, N - 2$ .

In Eq. (A2),

$$UR1 = -u_{i,j}^k \frac{1}{12 \Delta x} (x_1 - 8x_2 + 8x_3 - x_4), \quad UR2 = -\overline{v_{i,j}^k}^{xy} \frac{1}{12 \Delta x} (x_5 - 8x_6 + 8x_7 - x_8),$$

$$UR3 = -f_{i,j} \overline{u_{i,j}^k}^{xy}, \quad UR4 = -g \frac{1}{12 \Delta x} (x_9 - 8x_{10} + 8x_{11} - x_{12}),$$

$$UR5 = -\frac{C_f u_{i,j}^k}{\zeta_{i,j}^{k+1} + h_{i,j}} \left( (u_{i,j}^k)^2 + (\overline{v_{i,j}^{xy}})^2 \right), \quad UR6 = \frac{\tau_x}{\rho (\zeta_{i,j}^{k+1} + h_{i,j})},$$

$$x_1 = u_{i-2,j}^k, \quad x_2 = \overline{u_{i-1,j}^k},$$

$$x_3 = \begin{cases} \overline{u_{i+1,j}^k}, & \text{if } i \neq M-1, \\ 0.5(3u_{i,j}^k - u_{i-2,j}^k), & \text{otherwise,} \end{cases}$$

$$x_4 = \begin{cases} u_{i+2,j}^k, & \text{if } i \neq M-1, \\ (3u_{i,j}^k - 2u_{i-2,j}^k), & \text{otherwise,} \end{cases}$$

$$x_5 = u_{i,j-2}^k, \quad x_6 = \overline{u_{i,j-1}^k}, \quad x_7 = \overline{u_{i,j+1}^k}, \quad x_8 = u_{i,j+2}^k,$$

$$x_9 = \begin{cases} \overline{\zeta_{i-2,j}^{k+1}}, & \text{if } i \neq 3, \\ 0.5(3\zeta_{i-1,j}^{k+1} - \zeta_{i+1,j}^{k+1}), & \text{otherwise,} \end{cases}$$

$$x_{10} = \zeta_{i-1,j}^{k+1}, \quad x_{11} = \zeta_{i+1,j}^{k+1},$$

$$x_{12} = \begin{cases} \overline{\zeta_{i+2,j}^{k+1}}, & \text{if } i \neq M-1, \\ 0.5(3\zeta_{i+1,j}^{k+1} - \zeta_{i-1,j}^{k+1}), & \text{otherwise.} \end{cases}$$

Discretization of  $v$ -component of momentum equation is similar to that of the  $u$ -component and hence the discretized  $v$ -component of momentum equation is not presented here for the sake of brevity.

From the boundary conditions, given by Eqs (8)-(10), the elevations at  $j = 1$ ,  $j = N$  and  $i = M$  are computed, respectively, in the following manner:

$$\zeta_{i,1}^{k+1} = \zeta_{i,3}^{k+1} - 2\sqrt{\frac{h_{i,2}}{g}} v_{i,2}^k, \quad (A3)$$

$$\zeta_{i,N}^{k+1} = \zeta_{i,N-2}^{k+1} + 2\sqrt{\frac{h_{i,N-1}}{g}} v_{i,N-1}^k, \quad (A4)$$

$$\zeta_{M,j}^{k+1} = \zeta_{M-2,j}^{k+1} + 2\sqrt{\frac{h_{M-1,j}}{g}} u_{M-1,j}^k + 4a \sin\left(\frac{2\pi t}{T} + \varphi\right), \quad (A5)$$

where  $i = 2, 4, 6, \dots, M-2$  and  $j = 1, 3, 5, \dots, N$ .

Finally, Eq. (11) can be written in discretized form as

$$(u_b)_{1,j}^{k+1} = u_{3,j}^{k+1} + \frac{Q}{(\zeta_{3,j}^{k+1} + h_{3,j})B}, \quad (A6)$$

where  $j = 7, 9, 11, 13, 15, 17, 19$ .